Cytometry
PART A
Journal of the International Society for Advancement of Cytometry

Comparative Study of Human Erythrocytes by Digital Holographic Microscopy, Confocal Microscopy, and Impedance Volume Analyzer

Benjamin Rappaz,[1] Alexander Barbul,[2] Yves Emery,[3] Rafi Korenstein,[2] Christian Depeursinge,[4] Pierre J. Magistretti,[1,5] Pierre Marquet[1,5]*

[1]Brain Mind Institute, Ecole Polytechnique Fédérale de Lausanne, 1015 Lausanne, Switzerland

[2]Department of Physiology and Pharmacology, Sackler Faculty of Medicine, Tel Aviv University, Tel Aviv, Israel

[3]Lyncée Tec SA, PSE-A, 1015 Lausanne, Switzerland

[4]Laboratoire d'Optique Appliquée, Ecole Polytechnique Fédérale de Lausanne, 1015 Lausanne, Switzerland

[5]Département de psychiatrie DP-CHUV, Centre de Neurosciences Psychiatriques, Site de Cery, 1008 Prilly-Lausanne, Switzerland

Received 18 June 2007; Revision Received 15 February 2008; Accepted 29 May 2008

Additional Supporting Information may be found in the online version of this article.

Grant sponsor: Swiss National Science Foundation; Grant number: 205320-112195; Grant sponsor: CTI; Grant number: LSPP-LS 8421.1; Grant sponsor: Nano2Life European network of excellence in bionanotechnology

*Correspondence to: Pierre Marquet, Département de psychiatrie DP-CHUV, Centre de Neurosciences Psychiatriques, Site de Cery, 1008 Prilly-Lausanne, Switzerland

Email: p.marquet@a3.epfl.ch

ISAC
International Society for Advancement of Cytometry

Abstract

Red blood cell (RBC) parameters such as morphology, volume, refractive index, and hemoglobin content are of great importance for diagnostic purposes. Existing approaches require complicated calibration procedures and robust cell perturbation. As a result, reference values for normal RBC differ depending on the method used. We present a way for measuring parameters of intact individual RBCs by using digital holographic microscopy (DHM), a new interferometric and label-free technique with nanometric axial sensitivity. The results are compared with values achieved by conventional techniques for RBC of the same donor and previously published figures. A DHM equipped with a laser diode ($\lambda = 663$ nm) was used to record holograms in an off-axis geometry. Measurements of both RBC refractive indices and volumes were achieved via monitoring the quantitative phase map of RBC by means of a sequential perfusion of two isotonic solutions with different refractive indices obtained by the use of Nycodenz (decoupling procedure). Volume of RBCs labeled by membrane dye DiI was analyzed by confocal microscopy. The mean cell volume (MCV), red blood cell distribution width (RDW), and mean cell hemoglobin concentration (MCHC) were also measured with an impedance volume analyzer. DHM yielded RBC refractive index $n = 1.418 \pm 0.012$, volume 83 ± 14 fl, MCH = 29.9 pg, and MCHC 362 ± 40 g/l. Erythrocyte MCV, MCH, and MCHC achieved by an impedance volume analyzer were 82 fl, 28.6 pg, and 349 g/l, respectively. Confocal microscopy yielded 91 ± 17 fl for RBC volume. In conclusion, DHM in combination with a decoupling procedure allows measuring noninvasively volume, refractive index, and hemoglobin content of single-living RBCs with a high accuracy.

Key terms

digital holographic microscopy; laser scanning confocal microscopy; impedance volume analyzer; red blood cell volume; MCV; refractive index; mean corpuscular hemoglobin concentration; MCHC

MATURE erythrocytes (red blood cells, RBCs) represent the main cell type in circulating blood. They can be characterized by specific biconcave shape, high hemoglobin content, and absence of intracellular organelles such as the nucleus, mitochondria, or endoplasmic reticulum (1). Parameters such as RBC shape, volume, refractive index, and hemoglobin content are important characteristics that can be used as good indicators of the body's physiological state (2). For instance, erythrocyte volume distribution is altered in patients with anemia, folate and vitamin B_{12} deficiency, and microcytic anemia (2). The refractive properties of erythrocytes in diabetic patients differ significantly from those of healthy donors (3). Oxygen saturation also modulates the hemoglobin refractive index (4). Thus, monitoring the refractive index of erythrocytes can be used to assess their level of oxygen saturation. In addition, as the hemoglobin content is mainly responsible for the refractive index of the RBC, this

Published online 9 July 2008 in Wiley InterScience
(www.interscience. wiley.com)

DOI: 10.1002/cyto.a.20605

parameter can be used as a measure of the mean cell hemoglobin concentration (MCHC) (5).

The first effort to measure the erythrocyte refractive index was conducted by perfusing RBCs with solutions of increasing refractive index until the cells exhibit no contrast under the phase-contrast microscope (6). Using this technique, a refractive index of 1.386 was determined for living erythrocytes (7). Since then a few attempts were made to assess the refractive index of normal RBCs using different approaches yielding values ranging from 1.367 to 1.410 (6,8–11). To assess RBC volume, a few techniques have been implemented including light microscopy (12–14), impedance volume analysis (15), confocal fluorescence microscopy (16–19), light scattering (20,21) as well as packed cell volume (PCV) calculation (22). These studies determined the volume of normal individual erythrocytes to be 80–120 fl, depending on the technique employed.

Recently, a new emerging imaging approach, namely quantitative phase microscopy (QPM) has been demonstrated to provide accurate 3D imaging of transparent living cells (11,23–25). Although transparent specimens differ only slightly from their surrounding, in terms of optical properties, they have the capacity to induce wave front phase retardation on the transmitted wave. This natural phase retardation contrast, proportional to the thickness of the observed specimen, is a result of the difference in refractive indices between the specimen and the surrounding medium. Consequently, unlike traditional contrast-generating modes such as phase contrast (PhC), initially proposed by F. Zernike (26) or Nomarski's differential interference contrast (DIC) (27), QPM not only allows the visualization of transparent biological specimens but also provides quantitative information about both cell morphology and intracellular content related to the refractive index (25). The QPM technique we have developed, called digital holographic microscopy (DHM) is an interferometric approach based on the holographic principle (28). Briefly, from a single recorded hologram, quantitative phase images of living cells can be reconstructed by a numerical process (29). This numerical processing of holograms presents the great advantage of offering the means not only to reconstruct quantitative phase image but also to achieve a numerical compensation for aberration (30) and experimental noise (time drift, vibration, etc.). Consequently, although classical interferometric phase shift measurements are very sensitive to experimental noise (lens defects, vibrations, thermal drift, etc.), DHM allows to quantitatively measure phase shift corresponding to a fraction of the wavelength of the coherent light wave used, e.g., a few nanometers, with a high temporal stability and without using very demanding and costly opto-mechanical designs as required by conventional interferometric techniques. This explains why very few attempts to use conventional interferometric techniques have been reported in biology for real time living cell imaging. Nevertheless, interferometry was first used in 1957 by Barer (6) to measure refractive properties of RBC and later by Evans and Fung to measure erythrocyte dimensions (9).

As previously mentioned, the reconstructed quantitative phase image contains information about both the morphology and the refractive index of the monitored transparent specimen. As this dual information is intrinsically mixed, some strategies have been developed to separately assess the morphology and the refractive index. Kemper et al. (31) and Lue et al. (32) measured the cell integral refractive index by trapping cells between two cover glasses, whose distance apart is experimentally determined. On the other hand, a combined method has been proposed involving confocal microscopy to determine cell thickness and QPM to calculate the intracellular refractive index (33). We have developed a specific decoupling procedure, based on a concept initially proposed in (6,9), allowing to directly calculate from the quantitative phase signal the corresponding cell morphology and integral refractive index. This procedure is particularly useful for measuring, under the same experimental conditions, both cell morphology changes and associated integral refractive index modifications occurring during biological processes (34).

In this article, we demonstrate the applicability of the DHM technique, in combination with a decoupling procedure, for the precise measurements of refractive indices and volumes of intact individual erythrocytes. The obtained values of erythrocyte mean cell volume (MCV), refractive index, and mean corpuscular hemoglobin (MCH) and concentration (MCHC) are compared with values obtained by an impedance volume analyzer, a laser scanning confocal microscope, and reference values found in the literature.

Materials and Methods

Cell Preparation

RBCs were prepared according to Fairbanks (30), with small modifications (35). In short: 100–150 μl of blood was drawn from healthy laboratory personnel by fingerpick, collected, and diluted at a ratio of 1:10 (v/v) in cold HEP buffer (15 mM HEPES pH 7.4, NaCl 130 mM, KCl 5.4 mM, and 10 mM glucose). Blood cells were sedimented at 200*g*, 4°C for 10 min and buffy coat was gently removed. RBCs were washed twice in HEP buffer (1,000*g* × 2 min at 4°C). Finally, erythrocytes were suspended in HEPA buffer (15 mM HEPES pH 7.4, 130 mM NaCl, 5.4 mM KCl, 10 mM glucose, 1 mM $CaCl_2$, 0.5

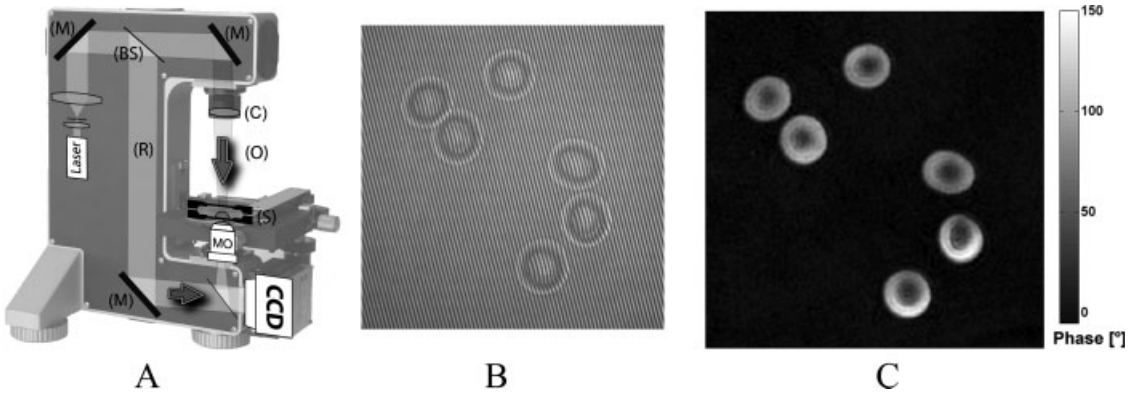

Figure 1. (**A**) Basic configuration for an inverted digital holographic microscopy (DHM). A VCSEL laser diode produces the coherent light (λ = 663 nm), which is divided by a 50/50 beam splitter (BS). The specimen (S) is illuminated by one beam through a condenser (C). A microscope objective (MO) collects the transmitted light and forms the object wave (O), which interferes with a reference beam (R) to produce the hologram recorded by the digital CCD camera. The sample is mounted in a closed perfusion chamber used to apply the different solutions; (M) mirrors. (**B**) Typical example of a hologram acquired by the camera (512 × 512 pixels). (**C**) Typical quantitative phase image of erythrocytes.

mM $MgCl_2$, and 1 mg/ml bovine serum albumin) at 0.2% hematocrit. The erythrocyte suspension was introduced into the experimental perfusion chamber consisting of two cover glasses separated by spacers 1.2 mm thick, and incubated for 20 min at 37°C. This allows the erythrocytes to adhere to the glass coverslip. Unattached cells were removed by gently perfusing the chamber with HEPA solution. The chamber was then mounted on the DHM stage, and holograms were acquired and numerically reconstructed online using a custom-made C++ software (36). Neither erythrocyte shape transitions nor volume changes were detected throughout the experiment. All experiments were conducted at room temperature (~22°C). For the decoupling procedure presented later, either 60 mM mannitol or 60 mM Nycodenz (HistoDenz™, Sigma) was added to the HEPA buffer. In addition, water was added to preserve the osmolarity of 298 mOsm (measured with a freezing-point osmometer (Roebling, Germany)). The perfusion chamber was placed in the setup about 1 h before imaging to prevent drifts (thermal or mechanical) during the recording period.

Digital Holographic Microscope Experimental Setup

The experimental setup is a modified Mach-Zehnder configuration (Fig. 1A). A vertical cavity surface emitting laser (VCSEL, Firecomms) is used to produce an illumination light at 663 nm. Light transmitted by the specimen and collected by a Nikon Plan Apo 60 × 0.95 NA microscope objective (MO) forms the object wave ***O***, which interferes with a reference wave ***R*** to produce the hologram intensity I_H recorded by the digital camera (Fig. 1B). Holograms are recorded in an off-axis geometry, i.e., the reference wave reaches the CCD camera (Basler A101f) with a small incidence angle (~1°) with respect to the propagation direction of the object wave. The pixel size on the camera (6.7 μm) corresponds to a size of 0.161 μm on the image plan.

A detailed description of the algorithm used for hologram reconstruction in such an off-axis configuration and aberration compensation have been previously described in (29,36).

Images were acquired at 1 Hz. The reconstruction process is achieved in real-time (>15 images/s) using a standard PC computer (Pentium IV, 3.2 GHz).

Decoupling Procedure

According to (34), the separate measurements of the integral refractive index ($\overline{n}_{c,i}$) and the cell thickness have been performed by measuring cell phase mapping, sequentially, in two iso-osmolar perfusion solutions of different refractive indices. Specifically, the refractive index of the second solution is increased by replacing mannitol (a hydrophilic sugar present in the standard perfusion solution) with equal molarity of the hydrophilic molecule Nycodenz. Typically, the addition of 4% w/v of Nycodenz increases the refractive index of the solution by $\delta_n = 0.006$. The different refractive indices have been precisely measured with a 2 WAJ Abbe refractometer at the wavelength of the VCSEL laser diode. Complementary experiments have shown an inertness and impermeability of mannitol and Nycodenz (data not shown).

The phase signal, for each pixel *i*, recorded with mannitol can be expressed as:

$$\varphi_{1,i} = \frac{2\pi}{\lambda}(\overline{n}_{c,i} - n_m)h_i \quad (1)$$

and with Nycodenz as:

$$\varphi_{2,i} = \frac{2\pi}{\lambda}(\overline{n}_{c,i} - (n_m + \delta n))h_i \quad (2)$$

where n_m and $n_m + \delta_n$ are the refractive indices of the two different perfusion solutions, h_i the cell thickness and $\overline{n}_{c,i}$ is the integral refractive index defined as the mean value of the intracellular refractive index along the cell thickness h_i (34). By solving this equation system, the $\overline{n}_{c,i}$ and h_i values, for each pixel *i*, are obtained.

However, to minimize the effect of erythrocyte submicromovements occurring over the 60 s solution exchange

time, the h_i values have been calculated by using, as a first approximation, the mean integral refractive index ($\overline{n}_c$) for each cell $\overline{n}_c = \frac{1}{N_c}\sum_{i=0}^{N_c} \overline{n}_{c,i}$ rather than $\overline{n}_{c,i}$ (34). As far as RBCs are concerned, the mean refractive index measurements of different erythrocyte regions do not present statistically significant spatial variations. Such a spatially homogeneous intracellular refractive index is consistent with a homogeneous erythrocyte cytoplasm containing no organelle and strengthens the appropriateness of the $\overline{n}_c$ approximation. The procedure of exchange of the extracellular medium was repeated three times to improve measurement accuracy. Each time the experimental chamber was perfused with ~100× the chamber volume to ensure complete solution exchange.

Confocal Laser Scanning Microscopy

The RBCs prepared in HEPA solution were incubated at 37°C for 20 min with 3 μl/ml of the lipophilic plasma membrane dye Vybrant Dil (Molecular Probes, excitation peak: 549, emission peak: 565) and washed twice in HEPA buffer before being mounted between two coverslips. The preparation was imaged with a Plan Apo 63x/1.3 NA glycerol immersion objective on an inverted Leica TCS-SP2 AOBS confocal laser scanning microscope. The preparation was illuminated with a 561-nm DPSS laser and the emission was collected between 580 and 700 nm. The lateral and axial sampling intervals were of 107 and 163 nm, respectively. Images were recorded in 12 bits format. The pinhole was set to 1 Airy unit. Images were deconvoluted using the Maximum Likelihood Estimation (MLE) algorithm in Huygens2 (Scientific Volume Imaging, Netherlands) with a theoretical point-spread function (PSF).

The *z*-stacks were converted to tiff 16 bits images and imported into ImageJ 1.38v (http://rsb.info.nih.gov/ij/ Wayne Rasband, NIH), for processing. Specifically, images were smoothed twice and converted to binary using the threshold option. The cytoplasm regions having a pixel value of zero (not stained by the membrane specific dye) were manually set to one. 3D erosion was also applied until the edge of the binarized stack best fit the maximum intensity of the fluorescent halo around the membrane. This was achieved with the 3D toolkit option Morphological Erode 3D (http://ij-plugins.sourceforge.net/ij-3D-toolkit.html). The cell projected area (sensor area covered by the cell) was determined in ImageJ by measuring the surface of the maximum intensity projection. Finally, the stacks were imported into Imaris 6.0 (Bitplane AG, Switzerland) to measure the volume with the isosurface tool. A second channel with the deconvoluted fluorescent data was added to visually check whether the surface correctly estimates the cell volume (cf. Fig. 3).

Impedance Volume Analyzer

The mean corpuscular volume (MCV) and RBC distribution width (RDW, a measure of the variation of the RBC volume) were measured with a Sysmex KX-21 Impedance volume analyzer, an apparatus commonly used in hematology laboratories to obtain complete blood count from patients. A 50-μl sample of whole blood was analyzed. The cells were suspended in the Cellpack PK-30l medium (Sysmex) and lysed with the Stromatolyser-WH medium (Sysmex) for the hemoglobin measurement. The stability of the apparatus was assessed before each experimental day by a calibration essay (Eightcheck-3WP, Sysmex).

The KX-21 quantifies the hemoglobin concentration by measuring the optical density of lysed erythrocytes and comparing it with a calibration curve of various concentrations of hemoglobin.

Quality Assurance

Digital holographic microscope. DHM as an interferometric method uses laser wavelength, which is rather constant, as an intrinsic standard. It is not sensitive to laser power instability. The low coherence laser source of DHM is used in conjunction with an interferential band-pass filter to ensure perfect stability and a precise wavelength, specified to a precision of 0.01°. To ensure quality holograms, special attention was paid to achieve high coherence between the object beam and the reference beam. For this purpose, the DHM-1000 is equipped with a motorized system allowing automatic correction of the length of the optical path of the reference arm. Automatic adjustments of the optical path's length as well as the illumination intensity ratio between the object arm and the reference arm were performed before each experiment and rechecked each hour. CCD camera settings (gain, shutter time, and grey level) were carefully chosen by analysis of the histogram of pixel values of the hologram to guarantee that the image intensity is within the CCD dynamic range without over- and under-exposed pixels.

The calibration of the DHM setup in XY dimensions was performed using USA Airforce standard (USAF 1951). The vertical calibration along Z-axis is intrinsically linked to the phase measurements. Overall performance of DHM was checked employing 6.42-μm polystyrene beads with refractive index = 1.59 (Spherotech, Libertyville IL). Diluted beads suspension in water was put onto a microscopic slide and dried. A drop of glycerol-based mounting media with refractive index of 1.46 (Vectashield, Vector Labs, USA) was layered up and the slide covered with glass coverslip. Results of DHM analysis of 68 beads are shown in Supplementary Figure 1. Averaged diameter in XY plane is 6.74 ± 0.75 μm (11.07%; mean ± standard deviation, STD) and 6.70 ± 0.67 μm (9.99%) in Z-direction (height deduced from the phase shift and the knowledge of the bead refractive index). A sphericity index is 1.005 ± 0.025 (2.46%). Small contamination of the sample with the beads of two other grades can be seen (Supplementary Fig. 1). The averaged XYZ bead diameter for the main peak is 6.49 ± 0.084 (1.29%), which is very close to the manufacturer data of 6.42 μm with STD of 2% determined by light scattering.

The stability of the experimental setup to XY drift was checked by analyzing center of mass position of individual beads as well as of individual RBCs employing Matlab-based software. In both cases, the center of mass maximal translation in X and Y direction did not exceed 0.7 pixel over 5-min recordings (data not shown).

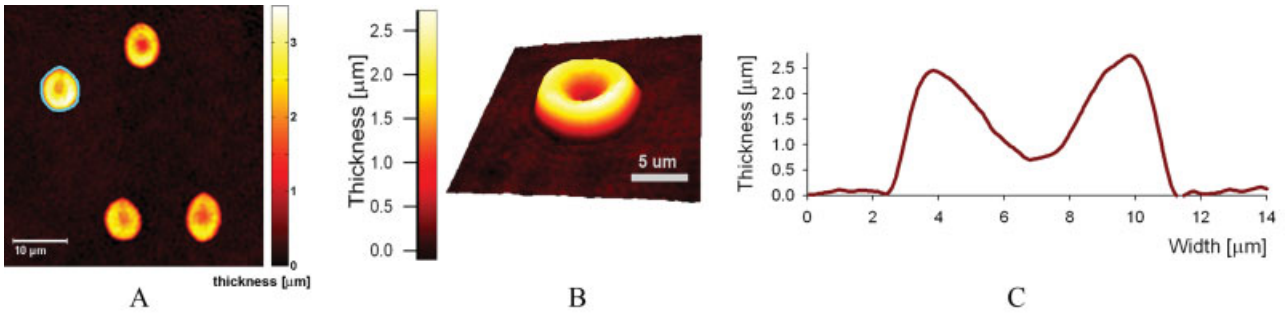

Figure 2. (**A**) Thickness distribution of human erythrocytes. The cell contour (light blue line) is determined by a classical gradient-based edge detection algorithm. The mean refractive index and the measured volume of selected cells are: $n = 1.396$ and $v = 99.3$ fl, respectively. (**B**) Pseudo 3D representation of the cell thickness of an erythrocyte (raw image). (**C**) Thickness profile obtained in central cross-section of the cell. [Color figure can be viewed in the online issue, which is available at www.interscience.wiley.com.]

Confocal laser scanning microscope. The quality assessment of our microscope was made according to the guideline provided in (37,38). If applicable, all tests were achieved in the same experimental conditions as the one used to image the RBC.

A homogenous field illumination was observed (by recording the image of a mirror) allowing to obtain a satisfactory stability during the 1 min recording time needed to image a single RBC. The stability of the light source spectrum (assessed with a HR2000 spectrometer, Ocean Optics) was also stable (less than 0.5 nm variation) during the typical recording period.

In addition, the vertical and horizontal stabilities of the scanner were assessed by measuring a grid pattern. Experimentally, no significant instability was observed in horizontal pattern, whereas a <100-nm shift was sometimes observed in vertical lines (due to the *x*-bidirectional scanning used to monitor RBC at a maximum speed to minimize cell movements).

The lateral resolution of our setup (at the 561 nm light source wavelength) was assessed by imaging 200 nm beads (Invitrogen). The full width at half maximum (FWHM) is of around 361 nm. The axial resolution was measured according to (37). We obtain a FWHM of around 464 nm. More details can be found in Supplementary Figures 2–6.

In addition to this one-time quality assessment, a performance check of the setup is routinely achieved. It consists in cleaning the microscope (microscope objective, filters, etc.), performing an optimization of the field illumination (Köhler illumination), and recording a point spread function of a 500-nm bead (Invitrogen), excited at 543 nm and recorded at 550–600 nm. Visual inspection of the recorded PSF and comparing it with a standard allows to monitor any changes in its shape (symmetry), reflecting a suboptimal microscope configuration.

Lastly, to ensure an optimal stability, the microscope and light source were turned-on 1.5–2 h before recording.

Impedance volume analyzer. A quality control of the Sysmex KX-21 is achieved before each day of experiments by a calibration assay. It consists in measuring a control blood sample (Eightcheck-3WP, Sysmex) and comparing the results with a normal range of value given by the manufacturer for eight parameters (WBC, RBC, HGB, HCT, MCV, MCH, MCHC, and PLT). If the results are outside this range, the apparatus needs to be calibrated.

The calibration procedure is achieved according to the recommendation of Sysmex KX-21 user guide. At least five samples of a healthy subject are used. Hemoglobin content (HGB) and hematocrit (HCT) of the subject are determined using another calibrated apparatus (recommended method: norm DIN 58931 for HGB and norm DIN 58933 for HCT). The blood samples are then measured with the Sysmex KX-21. At the end of the calibration procedure, any divergence between the results of the Sysmex and the other calibration apparatus are corrected by a compensation factor stored in the Sysmex software.

Results

DHM

Refractive indices of individual erythrocytes placed in the perfusion chamber were determined by employing the decoupling procedure and calculations based on Eqs. (1) and (2). RBC integral refractive index ($\bar{n}_c$) calculated over a sample of 36 erythrocytes was found to be 1.418 ± 0.012 (mean $\pm$ STD). From the knowledge of refractive indices of individual cells, one can easily translate phase signals into cell thickness (Fig. 2). This figure represents a typical DHM image of biconcave-shaped erythrocytes, 3D reconstruction of selected RBCs, as well as a thickness profile taken at the cell central cross-section.

Cell volumes have been estimated from morphometry images by the following expression:

$$V_c \cong \frac{S_{pixel}}{M^2} \sum_{i \in S_{cell}} h_i, \qquad (3)$$

where h_i is the cell thickness corresponding to pixel i, S_{pixel} is the pixel area of the reconstructed image, and M the DHM magnification. The summation is achieved over the erythrocyte-projected surface S_{cell} (sensor area covered by the cell). The determination of the erythrocyte contour and therefore of the pixels forming S_{cell} has been performed on individualized

Table 1. Results of the measurements of normal erythrocytes by different techniques

TECHNIQUE	VOLUME [fl]	SURFACE [μm^2]	DIAMETER [μm]	REFRACTIVE INDEX	MCH [pg/cell]	MCHC [g/l]	N
DHM							
Mean	83.3	46.7	7.7	1.418	29.9	362	
STD	13.7	5.9	0.5	0.012	4.4	40	36
Dif_t	5.7	–	–	0.006	–	7	
CLSM							
Mean	90.7	46.9	7.7	–	–	–	
STD	16.7	6.8	0.6	–	–	–	34
Impedance volume analyzer							
Mean	81.8	–	–	–	28.6	349	
RDW−SD/CV	40.8/12.7	–	–	–	–	–	$\sim 3 \times 10^5$

[a]DHM, digital holographic microscopy; CLSM, confocal laser scanning microscopy; impedance volume analyzer (Sysmex KX-21). *N*, number of cells; STD, standard deviation for cell population; Dif_t, averaged difference of individual cells for measurements taken at different times; RDW, red cell distribution width (expressed as coefficient of variation (CV, %) or standard deviation (SD, fL)).

erythrocytes by a classical gradient-based edge detection algorithm (blue line in Fig. 2A). Considering the effective lateral resolution of the microscope objective (0.5 μm) as well as the h_i measurement fluctuations, we obtain a volume estimation with an accuracy of ± 6 fl. The erythrocyte diameter (d) has been estimated by considering the diameter of the circle having the erythrocyte area,

$$d \cong \frac{2}{M}\sqrt{\frac{S_{cell}}{\pi}}. \quad (4)$$

Taking into consideration the DHM lateral resolution, the precision of the measured S_{cell} is of $\sim 9\ \mu m^2$. Table 1 presents the mean and standard deviation of the erythrocyte volume, the diameter, and the intracellular integral refractive index ($\overline{n}_c$) calculated over a sample of 36 erythrocytes. The third line shows the mean temporal difference (Dif_t) over the considered RBC sample, defined as the absolute difference of the considered parameter calculated with the DHM on a set of two values measured 3 min apart on the same cell. It may be seen that measurements are rather stable with Dif_t being much less than STD, determined by intercellular differences.

Calculation of Hemoglobin Content

In the case of RBCs, which are mainly composed of hemoglobin, the phase signal can be directly related to the mean corpuscular hemoglobin (MCH) as proposed by Barer (39).

$$\mathrm{MCH} = \frac{10\varphi\lambda S_{cell}}{2\pi\alpha_{Hb}}, \quad (5)$$

where φ is the mean phase shift induced by the whole cell, λ is the wavelength of the light source of the setup (663 nm), S_{cell} is the projected cell surface, and $\alpha_{Hb} = 0.00196$ dl/g is the hemoglobin refraction increment at 663 nm. This formula allows to directly and noninvasively measure the MCH of single RBC (without using the decoupling procedure). The experimentally measured MCH is 29.9 pg/cell ($n = 36$).

Knowledge of the MCV, obtained with the decoupling procedure, allows to calculate the MCHC of individual red cells by dividing MCH by MCV. A mean MCHC value of 362 g/l is obtained.

Confocal Laser Scanning Microscopy

Figure 3 shows a typical isosurface rendering of an erythrocyte imaged with the confocal laser scanning microscope after deconvolution, allowing to observe, in particular, the typical biconcave shape corresponding to a healthy cell shape.

The cell diameter has been calculated by Eq. (4), where S_{cell} is taken from the binarized confocal z-slice located at the mean height of the cell. Table 1 presents the mean and standard deviation of erythrocyte volume as well as the diameter calculated over a 34-erythrocytes sample with the confocal microscope. The precision of volume estimation is mainly affected by the deconvolution procedure, the resolution of the setup, and the spreading of the fluorescent halo around the membrane of the cell (Fig. 3). Considering these effects, we are able to measure erythrocyte volume with an accuracy of about 25%.

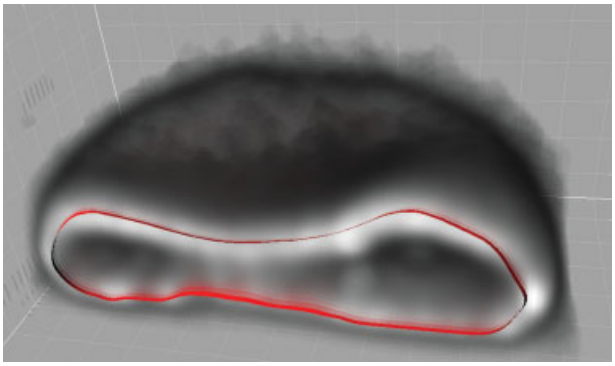

Figure 3. XZ cut into the 3D distribution of the fluorescent intensity after deconvolution (gray) showing the isosurface inside it (black [red in online color version]). The surface closely follows the maximum of intensity of the fluorescent dye DiI incorporated into the erythrocyte membrane. The measured volume and diameter of this cell are 113 fl and 7.6 μm, respectively. [Color figure can be viewed in the online issue, which is available at www.interscience.wiley.com.]

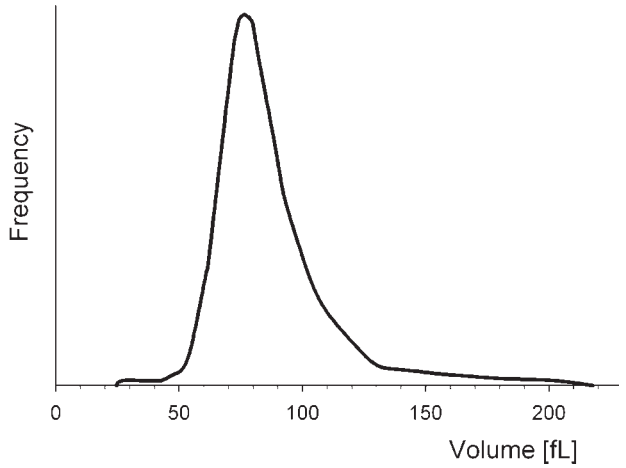

Figure 4. A representative frequency distribution of erythrocytes volumes measured with the Sysmex KX-21 impedance volume analyzer. MCV = 81.9 fl, RDW−SD = 40.7 fl, RDW-CV (graphically obtained) 12.7%.

Impedance Volume Analyzer

The distribution of erythrocyte volumes was measured by electronic cell counting (n = 6 samples of ~50,000 cells each). Because of the large number of cells analyzed, this technique allows to obtain the RBC volume distribution curve (Fig. 4). The presence of a single peak indicates the existence of a homogeneous erythrocyte population. The values obtained with the Sysmex KX-21 Impedance volume analyzer are as follows: MCV = 82 fl, RDW-SD (standard deviation) = 41 fl, and RDW-CV (coefficient of variation) = 12.7% (Table 1). The optically measured MCH and MCHC obtained with the Sysmex KX-21 are 28.6 pg/cell and 348 g/l, respectively.

Discussion

DHM quantitatively measures optical phase shift, which provides quantitative information about both cell morphology and intracellular content related to the refractive index. Because of its high phase sensitivity and temporal stability, DHM enables the monitoring of fine dynamic processes in a living material with a great ease of use (25). In this study, we exploited such advantages to measure the refractive index of intact human RBC with a high accuracy.

Although the refractive index seems to be very sensitive to pathological alterations and thus to be important in diagnostics (3), only few attempts were previously made to assess this parameter. The situation may be explained by the complexity and inaccuracy of existing approaches. For example, the approach of Barer (6) involves an arbitrary judgment of the point when the erythrocytes sample and the solution of high concentration of albumin with n = 1.386 exhibit minimum contrast under the phase microscope. Others (9) directly measured the hemolyzed content of erythrocytes or the refractive index of packed cells. However, in both cases RBCs were far from their native state. Ghosh et al. (8) had found n = 1.405 and 1.410 for two normal volunteers by analyzing the angular dependence of laser light scattering from dense RBCs preparations. This approach uses the isovolumetrical sphering of RBCs due to difficulties in calculating light scattering from a biconcave discoid RBC. However, the procedure of sphering (40) itself can introduce artifacts. Defocusing microscopy (10) raised the value of $n = 1.381 \pm 0.005$ for human RBC, but this technique requires exact knowledge of the RBC's height. Curl et al. (11) used a hypotonic agent to sphere the rat RBCs and measure their refractive index (n = 1.367) by QPM. This approach could underestimate the refractive index as the hypotonic shock causes a water entry into the cell. The value of n = 1.418, which we report in this work, is in the range of previously reported values but should be more precise as minimal RBC perturbation was employed and measurements were performed with high accuracy.

Another important RBC parameter, the cell volume, can be estimated as PCV-packed cell volume (22). In this approach, RBCs are subjected to prolonged 30 min centrifugation under relatively high centrifugal acceleration of 1,200–2,500*g*. To correct measurements for entrapped water, a radioactive label should be added for precise determinations (41). The volume of individual erythrocytes can be calculated by dividing the PCV by RBC count that generally yields a value of 90 fl. Such approach is laborious and time consuming, and alternative flow cytometry techniques are used now in the routine laboratory practice. One such flow cytometry technique is based on the detection of changes in electrical resistance produced by nonconductive particles such as cells suspended in an electrolyte when they pass through a narrow orifice (Coulter principle, (15)).

Another flow cytometry approach is to measure the amount of light scattered by individual red cells flowing through a narrow sensing aperture (20,21); this technique allows for the independent measurement of the cell volume and mean hemoglobin concentration derived from the mean refractive index. On the other hand, one of the most sophisticated ways of estimating single cell volume is by confocal laser scanning microscopy (CLSM) (16–19). Indeed, the use of lipophilic fluorescent dyes to generate a specific cell membrane contrast or observation of autofluorescence and digital image processing of the image sets, consisting of serial optical sections across the cell, allows obtaining a 3D model of an individual cell. In particular, volume and shape estimation of living RBC have been obtained (42).

Figure 5 compares the results of volume measurements performed on the blood samples from the same healthy donor achieved by different techniques: Box plot distribution obtained with Sysmex KX-21 impedance volume analyzer (extrapolated from Fig. 4), CLSM and DHM, as well as some results from previous studies and the typical textbook value of 92 ± 9 fl (22) are indicated.

Figure 5 shows good agreement between results obtained by DHM and with the impedance volume analyzer. Results obtained by confocal microscopy are slightly higher, as results obtained in the literature with similar techniques such as light microscopy or CLSM. For example, Jay (12) using the approach described in (14), based on photographing individual RBCs hanging on edge, reports a typically MCV of 104.2.

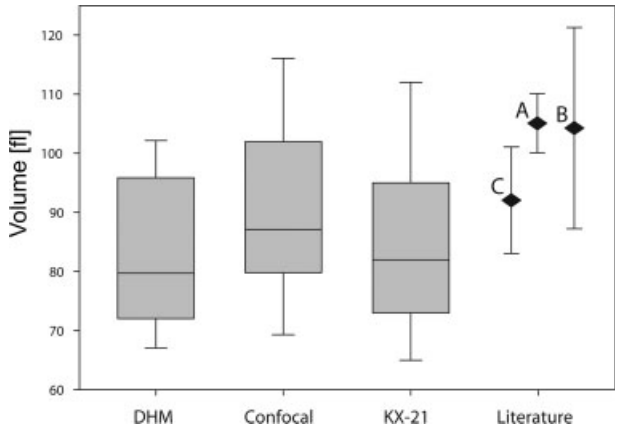

Figure 5. Box plot representation of the volume distribution obtained according to the method used. The box represents the median and the 25th and 75th percentile of the values, the whiskers represent the 10th and 90th percentile. DHM, digital holographic microscope ($n = 36$); confocal, Leica TCS-SP2 AOBS confocal laser scanning microscope ($n = 34$); KX-21, Sysmex KX-21 (6 measurements). References values from the literature are from (**A**) bright-field microscope (12) and (**B**) confocal microscope (42). (**C**) (22) is a textbook reference value.

Difato et al. (42) obtained a value of 105 ± 5 fl for fixed RBCs by means of confocal microscopy and deconvolution procedures for calculations. The higher MCV values obtained with these techniques compared to DHM and impedance volume analyzer can be explained by the difficulty to precisely determine the cell edge and the need to use delicate deconvolution and analysis procedure (as described in this article and in (42)).

In Coulter sizing instruments, the magnitude of the resistive pulse generated by a cell depends not only on the cell volume but also on the cell shape. Rod-like particles traversing the instrument's orifice are thought to rise an electric pulse of "ideal" form, whereas signals obtained from spherical or disk-like particles need to be corrected by a shape factor (43). The shape dependence is even more complicated by the deformation the cells undergo while traversing the aperture (44). Thus, cytoplasmic viscosity (dependent on hemoglobin concentration in RBC) significantly influences cell deformation. Therefore, erythrocyte volume measurements are affected by hemoglobin concentrations, a quantity that varies from one cell to another (45). The parameters used for the measurement including dimensions of aperture and magnitude of electrical current also influence the shape of the volume distribution measured (46), for instance pulses from cells whose trajectories are close to the orifice can artificially broaden the volume distribution of the high volume side (as observed in Fig. 4). In practice, Coulter instruments are calibrated (47) by means of latex beads to obtain values for RBC mean cell volume close to that obtained by PCV. The same is true with another flow cytometry approach based on the light scattering by individual red cells flowing through a narrow sensing aperture. In this approach, the cells have to undergo an unphysiological isovolumetric spheric change before measurement (40). As PCV determination implies long and relatively strong centrifugation, the RBC can lose part of its water and the resulting MCV may be less than for intact unstressed RBC as suggested previously (13).

Concerning the hemoglobin content measurement, the MCHC results obtained with DHM (362 ± 7 g/l, mean ± standard error of the mean) are in good agreement with those obtained with the impedance volume analyzer (349 ± 12 g/l, mean ± accuracy given by the manufacturer). The Sysmex KX-21, which compares the optical density of lysed erythrocytes versus a calibration curve, allows to obtain a very precise measurement of the MCHC of cell populations and provides high throughput but is highly invasive as cell lysis is required. On the contrary, DHM measures the hemoglobin concentration of individual cells in a manner that is independent on the shape and state of the cell. The ability of DHM to measure the MCHC of erythrocytes independently and accurately may allow for the objective evaluation of the biological variation of this parameter in various RBC disorders such as anemia.

DHM is a new challenging interferometric imaging technique. In combination with the decoupling procedure, it allows to establish noninvasively the volume and intracellular refractive index of living cells with high accuracy. Specifically, the DHM measurements of erythrocyte volume and refractive index are in good agreement with data obtained by the more traditional techniques. Unlike flow cytometry, DHM does not currently exhibit high throughput capabilities but allows monitoring and measuring parameters (morphology, refractive index, MCHC) of individual erythrocytes. Further developments of the DHM technique, by applying automatic algorithms of analysis and increasing output capabilities, may promote it as the method that reveals subpopulations based on the parameters measured at a single cell level. On the other hand, DHM permits online tracking of changes in individual cells during, for example, osmotic fragility test or shear stress. It does not require utilization of fluorescent probes and employing of delicate and time-consuming deconvolution and image analysis procedures such as CLSM. Using DHM, the intracellular hemoglobin content of individual cells, a parameter altered in various pathological states, can be directly estimated from the phase measurements.

Acknowledgments

The authors would like to thank Thierry Laroche and Juan-Carlos Floyd Sarria from the BioImaging and Optics platform at the EPFL and Arnaud Paradis from the CIF imaging facility for their technical assistance in the confocal experiments.

Literature Cited

1. Mazeron P, Muller S, ElAzouzi H. Deformation of erythrocytes under small-angle light scattering study. Biorheology 1997;34:99–110.
2. Bessman JD, Johnson RK. Erythrocyte volume distribution in normal and abnormal subjects. Blood 1975;46:369–379.
3. Mazarevica G, Freivalds T, Jurka A. Properties of erythrocyte light refraction in diabetic patients. J Biomed Opt 2002;7:244–247.
4. Faber DJ, Aalders MCG, Mik EG, Hooper BA, van Gemert MJC, van Leeuwen TG. Oxygen saturation-dependent absorption and scattering of blood. Phys Rev Lett 2004;93:028102.

5. Barer R, Joseph S. Refractometry of living cells. I. Basic principles. Q J Microsc Sci 1954;95:399–423.
6. Barer R. Refractometry and interferometry of living cells. J Opt Soc Am 1957;47:545–556.
7. Thaer A. The refractive index and dry mass distribution of mammalian erythrocytes. J Microsc 1969;89:237–250.
8. Ghosh N, Buddhiwant P, Uppal A, Majumder SK, Patel HS, Gupta PK. Simultaneous determination of size and refractive index of red blood cells by light scattering measurements. Appl Phys Lett 2006;88:084101.
9. Evans E, Fung YC. Improved measurements of erythrocyte geometry. Microvasc Res 1972;4:335–347.
10. Mesquita LG, Agero U, Mesquita ON. Defocusing microscopy: An approach for red blood cell optics. Appl Phys Lett 2006;88:133901.
11. Curl C, Bellair C, Harris P, Allman B, Roberts A, Nugent K, Delbridge L. Single cell volume measurement by quantitative phase microscopy (QPM): A case study of erythrocyte morphology. Cell Physiol Biochem 2006;17:193–200.
12. Jay AWL. Geometry of human erythrocyte. I. Effect of albumin on cell geometry. Biophys J 1975;15:205–222.
13. Canham PB, Burton AC. Distribution of size and shape in populations of normal human red cells. Circ Res 1968;22:405–422.
14. Ponder E. The measurement of the diameter of erythrocytes. V. The relation of the diameter to the thickness. Q J Exp Physiol 1930;20:29–39.
15. Coulter WH. High speed automatic blood cell counter and cell size analyser. Proc Natl Electron Conf 1956;12:1034–1042.
16. Errington RJ, Fricker MD, Wood JL, Hall AC, White NS. Four-dimensional imaging of living chondrocytes in cartilage using confocal microscopy: A pragmatic approach. Am J Physiol Cell Physiol 1997;41:C1040–C1051.
17. Zhu QZ, Tekola P, Baak JPA, Belien JAM. Measurement by confocal laser-scanning microscopy of the volume of epidermal nuclei in thick skin sections. Anal Quant Cytol Histol 1994;16:145–152.
18. Crowe WE, Altamirano J, Huerto L, Alvarezleefmans FJ. Volume changes in single N1e-115 neuroblastoma-cells measured with a fluorescent-probe. Neuroscience 1995;69:283–296.
19. Guilak F. Volume and surface-area measurement of viable chondrocytes in-situ using geometric modeling of serial confocal sections. J Microsc (Oxford) 1994;173:245–256.
20. Tycko DH, Metz MH, Epstein EA, Grinbaum A. Flow-cytometric light-scattering measurement of red blood-cell volume and hemoglobin concentration. Appl Opt 1985;24:1355–1365.
21. Mohandas N, Kim YR, Tycko DH, Orlik J, Wyatt J, Groner W. Accurate and independent measurement of volume and hemoglobin concentration of individual red-cells by laser-light scattering. Blood 1986;68:506–513.
22. Lewis SM, Bain BJ, Bates I. Dacie and Lewis Practical Haematology, 9th ed. London: Churchill Livingstone; 2001. 633 p.
23. Carl D, Kemper B, Wernicke G, von Bally G. Parameter-optimized digital holographic microscope for high-resolution living-cell analysis. Appl Opt 2004;43:6536–6544.
24. Popescu G, Ikeda T, Best CA, Badizadegan K, Dasari RR, Feld MS. Erythrocyte structure and dynamics quantified by Hilbert phase microscopy. J Biomed Opt 2005; 10:060503.
25. Marquet P, Rappaz B, Magistretti PJ, Cuche E, Emery Y, Colomb T, Depeursinge C. Digital holographic microscopy: A noninvasive contrast imaging technique allowing quantitative visualization of living cells with subwavelength axial accuracy. Opt Lett 2005;30:468–470.
26. Zernike F. Phase contrast, a new method for the microsopic observation of transparent objects. Physica 1942;9:686–698.
27. Nomarski G. Nouveau dispositif pour l'observation en contraste de phase differentiel. J Phys Radium 1955;16:S88–S88.
28. Gabor D. A new microscopic principle. Nature 1948;161:777–778.
29. Cuche E, Marquet P, Depeursinge C. Simultaneous amplitude-contrast and quantitative phase-contrast microscopy by numerical reconstruction of Fresnel off-axis holograms. Appl Opt 1999;38:6994–7001.
30. Fairbanks G, Steck TL, Wallach DFH. Electrophoretic analysis of major polypeptides of human erythrocyte membrane. Biochemistry 1971;10:2606–2617.
31. Kemper B, Carl D, Schnekenburger J, Bredebusch I, Schafer M, Domschke W, von Bally G. Investigation of living pancreas tumor cells by digital holographic microscopy. J Biomed Opt 2006;11:34005.
32. Lue N, Popescu G, Ikeda T, Dasari RR, Badizadegan K, Feld MS. Live cell refractometry using microfluidic devices. Opt Lett 2006;31:2759–2761.
33. Curl CL, Bellair CJ, Harris T, Allman BE, Harris PJ, Stewart AG, Roberts A, Nugent KA, Delbridge LM. Refractive index measurement in viable cells using quantitative phase-amplitude microscopy and confocal microscopy. Cytometry A 2005;65A:88–92.
34. Rappaz B, Marquet P, Cuche E, Emery Y, Depeursinge C, Magistretti PJ. Measurement of the integral refractive index and dynamic cell morphometry of living cells with digital holographic microscopy. Opt Expr 2005;13:9361–9373.
35. Barbul A, Zipser Y, Nachles A, Korenstein R. Deoxygenation and elevation of intracellular magnesium induce tyrosine phosphorylation of band 3 in human erythrocytes. FEBS Lett 1999;455:87–91.
36. Colomb T, Montfort F, Kuhn J, Aspert N, Cuche E, Marian A, Charriere F, Bourquin S, Marquet P, Depeursinge C. Numerical parametric lens for shifting, magnification, and complete aberration compensation in digital holographic microscopy. J Opt Soc Am A Opt Image Sci Vis 2006;23:3177–3190.
37. Zucker RM. Quality assessment of confocal microscopy slide based systems: Performance. Cytometry A 2006;69A:659–676.
38. Zucker RM. Quality assessment of confocal microscopy slide-based systems: Instability. Cytometry A 2006;69A:677–690.
39. Barer R. Interference microscopy and mass determination. Nature 1952;169:366–367.
40. Kim YR, Ornstein L. Isovolumetric sphering of erythrocytes for more accurate and precise cell-volume measurement by flow-cytometry. Cytometry 1983;3:419–427.
41. IN ICFS, SIZING HEPOBC. Recommendation for reference method for determination by centrifugation of packed cell volume of blood. International Committee for Standardization in Haematology Expert Panel on Blood Cell Sizing. J Clin Pathol 1980;33:1–2.
42. Difato F, Mazzone F, Scaglione S, Fato M, Beltrame F, Kubinova L, Janacek J, Ramoino P, Vicidomini G, Diaspro A. Improvement in volume estimation from confocal sections after image deconvolution. Micros Res Tech 2004;64:151–155.
43. Thom R. Automated red cell analysis. Baillieres Clin Haematol 1990;3:837–850.
44. Bator JM, Groves MR, Price BJ, Eckstein EC. Erythrocyte deformability and size measured in a multiparameter system that includes impedance sizing. Cytometry 1984;5:34–41.
45. Arnfred T, Kristensen SD, Munck V. Coulter-counter model-S and model-S-plus measurements of mean erythrocyte volume (Mcv) are influenced by the mean erythrocyte hemoglobin concentration (Mchc). Scand J Clin Lab Invest 1981;41:717–721.
46. Bull BS. On distribution of red cell volumes. Blood 1968;31:503–515.
47. England JML, Mitchell S, Lloyd E, Rowan RM. Calibration and maintenance of semi-automated haematology equipment/prepared on behalf of the Unit of Health Laboratory Technology and Blood Safety, World Health Organization, Geneva. Geneva: World Health Organization; 1993. Report no WHO/LBS/92.8.